# Hole migration and optically induced charge depletion in GaSb/GaAs wetting layers and quantum rings

P. D. Hodgson,[1,*] R. J. Young,[1] M. Ahmad Kamarudin,[1,2] Q. D. Zhuang,[1] and M. Hayne[1]
[1]*Department of Physics, Lancaster University, Lancaster LA1 4YB, United Kingdom*
[2]*Department of Physics, Universiti Putra Malaysia, 43400 UPM Serdang, Selangor Darul Ehsan, Malaysia*
(Received 1 May 2013; revised manuscript received 25 July 2013; published 28 October 2013)

We present the results of photoluminescence (PL) measurements on a type-II GaSb/GaAs quantum dot/ring sample as a function of temperature (2 to 400 K) and over six orders of magnitude of incident laser excitation power. Optically induced charge depletion (OICD) was seen in both the wetting layer (WL) and quantum dots/rings but with remarkably different temperature dependent behavior. Holes originating from background acceptors migrate out of the WL as the sample temperature is raised to 30 K, while the onset of a blueshift in the PL from quantum rings, signaling their thermally induced charging with holes, is only observed at temperatures above 300 K. The presence of dark dots as a hidden reservoir for acceptor holes at the intermediate temperatures is proposed to explain this anomalous behavior. Due to the deep localization potential of GaSb/GaAs, thermalization of acceptor holes between dark dots and bright rings only occurs above room temperature. A rate equation model is presented which successfully replicates the main features of OICD observed here and in previous reports.

DOI: 10.1103/PhysRevB.88.155322 PACS number(s): 78.20.−e, 78.30.Fs, 78.55.−m

## I. INTRODUCTION

The unique properties of type-II self-assembled quantum dots (QDs) and quantum rings (QRs) offer many exciting possibilities for device fabrication and fundamental physical research. Numerous studies have already been carried out on their type-I counterparts, which have shown benefits over bulk devices due to the reduced dimensionality of these zero-dimensional structures. These benefits include higher thermal stability and lower threshold currents in lasers[1] and insensitivity to edge states in solar cells.[2] Furthermore, QDs have much potential for use in emerging fields such as quantum information processing.[3]

In type-II heterostructures such as the GaSb/GaAs nanostructures studied here, the carrier species are spatially separated and generally have a reduced recombination rate when compared to type-I heterostructures. This property makes GaSb/GaAs QD/QRs candidates for use in solar cells.[4,5] Large confinement energies,[6,7] negligible charging barriers,[8] and strong three-dimensional carrier confinement in GaSb/GaAs QD/QRs make them promising for use in memory devices.[9,10] The Aharanov-Bohm effect has already been observed in other type-II QD systems,[11,12] and the large confinement potential of GaSb/GaAs QD/QRs makes them a favorable candidate for observation of such effects at elevated temperatures.[13] Mott transitions are also of fundamental physical interest and are already known to occur in the GaSb/GaAs QD system.[14]

Strong blueshifts of emission energy with increasing excitation power are regularly seen in type-II systems. Capacitive charging,[15–17] band bending,[18–23] and state filling[24] are commonly used to explain the blueshift of the type-II QD/QR emission energy. But capacitive charging is believed to be dominant in the sample investigated here.[25,26] All of these mechanisms rely on increasing carrier density and/or dot occupancy to describe the observed blueshifts. However, in a few cases, redshifts of the QD emission energy with increasing laser power have been seen and explained by optically induced charge depletion (OICD).[27]

This paper details the results of a study into OICD in a GaSb/GaAs QD/QR sample. OICD was first seen in the two-dimensional electron gas of $\delta$-doped GaAs/AlGaAs quantum wells[28] and heterojunctions[29] and then later in type-II QDs.[27] Here we present the unique result of OICD in both the wetting layer (WL; at low temperature) and QD/QRs (above room temperature). This remarkable observation allows the temperature induced migration of holes to different nanostructures to be observed.

## II. OPTICALLY INDUCED CHARGE DEPLETION

Optically induced charge depletion is a process involving the interaction of photogenerated carriers, a quantum-confining nanostructure (QN) and dopants [Fig. 1(a)], resulting in the counterintuitive discharging of a nanostructure with increasing laser excitation power. This discharging is manifested as a redshift of the nanostructure's emission energy in PL measurements. For the type of structure discussed here, the acceptor holes preferentially occupy the QN (WL, QDs, or QRs) in the absence of laser excitation [1 in Fig. 1(b)]. At low laser powers the recombination rate in the QN is low, as there are few electrons present, and the QN occupancy remains high. As the laser power is raised, the number of electrons increases, and the recombination rate increases, reducing the QN occupancy [see 2 in Fig. 1(b)]. At the same time, the photogenerated holes occupy the acceptor states, which delay them reaching the QN. When the laser power, and thus the carrier photogeneration rate, is high enough, the acceptor states begin to become saturated [see 3 in Fig. 1(b)]. The excess photogenerated holes spill over into the QN, and any further increases to the laser power results in a blueshift of the emission energy [see 4 in Fig. 1(b)]. Effectively, the acceptor states act as a perturbation to the sample's behavior: At low laser powers the photogenerated carrier density is comparable to the acceptor density and unusual effects are seen, but at high laser power the photogenerated carrier density is much greater than the acceptor density and they no longer perturb the system.

 ©2013 American Physical Society

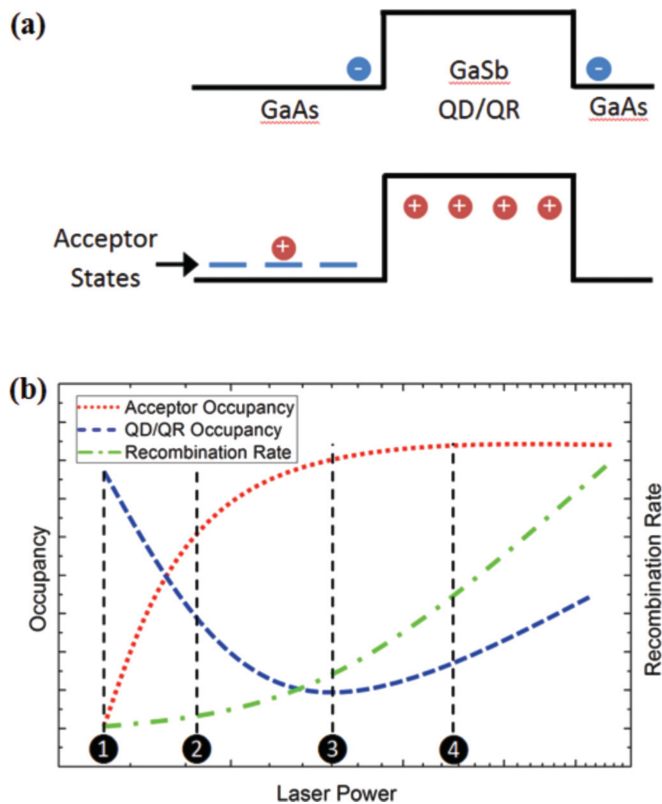


FIG. 1. (Color online) (a) Schematic bandgap diagram showing carrier locations at low laser powers (i.e., between 1 and 3). (b) Graphical illustration of the recombination rate of holes in the QDs with electrons in the GaAs; the hole occupancy of acceptor states and the hole occupancy of QD/QRs as a function of laser power. The main text gives a detailed explanation of how these effects lead to OICD.

## III. SAMPLE AND EXPERIMENTAL DETAILS

The sample was grown by molecular beam epitaxy (MBE) on a (100) GaAs substrate.[30] First a buffer layer of GaAs was grown at a temperature of 580 °C, followed by the deposition of 2.1 monolayers of GaSb at 490 °C with a V/III ratio of 2. An initial 9-nm cold cap was then grown at 430 °C and capped further by 100 nm of GaAs at 500 °C. Finally, a layer of GaSb was deposited under the same conditions as the first layer, allowing microscopy of the uncapped QD structures. Atomic force microscopy measurements of the surface of the sample revealed the presence of QDs with a lateral size of $43 \pm 7$ nm, height of $2.6 \pm 0.8$ nm, and density of $2.0 \times 10^{10}$ cm$^{-2}$ (Ref. 30). Cross-sectional transmission electron microscopy (XTEM) measurements of the subsurface GaSb structures showed both single- and double-lobed structures, believed to be QDs and QRs, respectively. The formation of QRs in GaSb/GaAs structures is often seen after capping and is believed to result from Sb migration away from the highly strained QD centers.[31]

Photoluminescence (PL) measurements were carried out in a continuous-flow Oxford Instruments cryostat at temperatures between 2 and 400 K. A 532-nm continuous-wave laser provided illumination to ∼2 mm$^2$ of the sample via a 200-$\mu$m-core optical fiber, allowing the power density to range from $\sim 10^{-2}$ to $10^4$ mW/cm$^2$. PL emission was collected by a

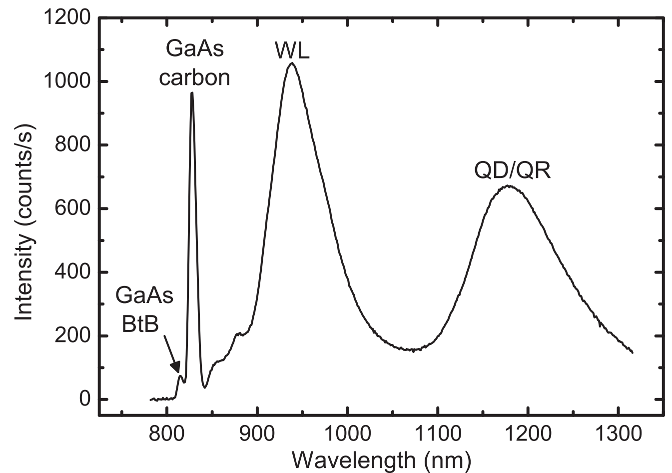


FIG. 2. PL spectrum at 2 K with a laser power of 29 mW/cm$^2$. Peaks, from left, are GaAs band-to-band (BtB), GaAs carbon-related peak, WL, and QD/QR.

550-$\mu$m-core optical fiber for measurement by a spectrometer and a Peltier-cooled InGaAs array.

## IV. RESULTS

Several emission peaks from the sample can be seen in Fig. 2. These peaks originate from the GaAs, GaSb QD/QRs, and WL. For reasons that shall be explained later, we believe that the QD/QR peak is strongly dominated by recombination from QRs, and for clarity we shall henceforth simply refer to it as the QR peak. Importantly, there is a strong emission peak at low temperatures with energy 23 meV lower than the band-to-band GaAs emission peak. This energy difference is consistent with carbon acceptor states above the GaAs valence band edge,[32] resulting from the unintentional incorporation of carbon atoms into the GaAs matrix during MBE growth. The WL peak quenches rapidly with increasing temperature and is not visible above 150 K. However, the QR peak is still visible at the 400 K limit of our equipment, even at low laser powers. This is unexpected for type-II structures, where the small electron-hole wave-function overlap gives weaker emission, especially at high temperatures. The strong high-temperature QR emission is important as it allowed observation of interesting effects, as described later.

Figure 3(a) shows the WL emission energy as the laser excitation power was varied at several different temperatures. At 2 K, a distinctive U-shaped dependence is seen,[27] with an initial redshift caused by OICD, followed by the common blueshift with increasing laser power. As the temperature is raised, the magnitude of the initial redshift decreases, until 20 to 30 K, when only a blueshift is observed. The more acceptor holes that are initially present in the WL, the greater the incident laser power needed to fully remove them, and the greater the initial redshift will be. Therefore, this result shows that the acceptor holes preferentially occupy the WL at low temperature and escape by thermal excitation as the temperature is increased. When the temperature has reached ∼30 K the majority of the acceptor holes have been excited out of the WL and a monotonic blueshift is seen.

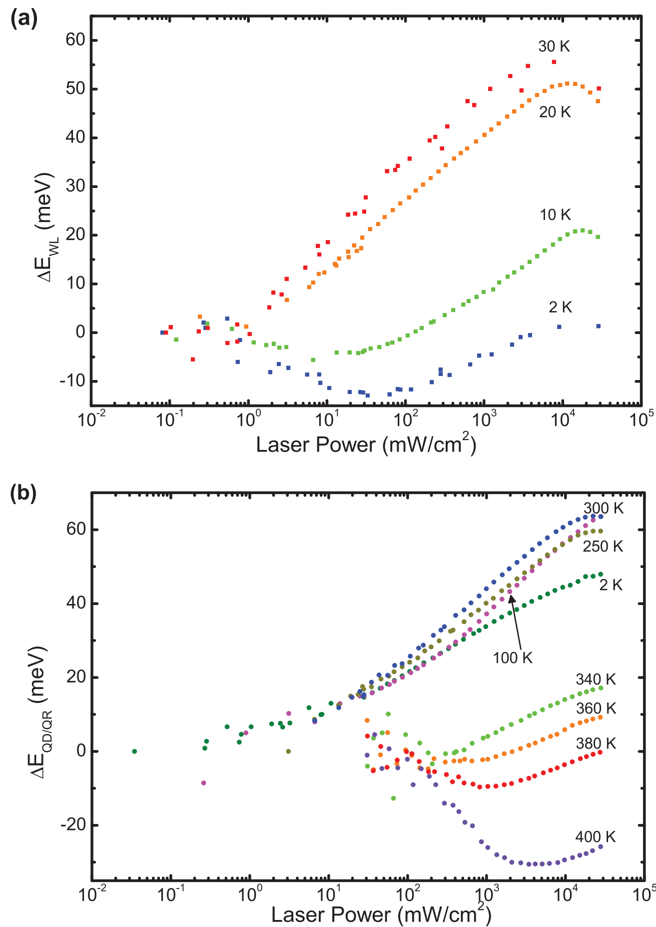


FIG. 3. (Color online) The PL emission energy shift for (a) the WL and (b) QR peaks with incident laser power density. The energies of data points are shifted so that the lowest power data point is roughly at zero energy (power scans at some temperatures have been omitted for clarity).

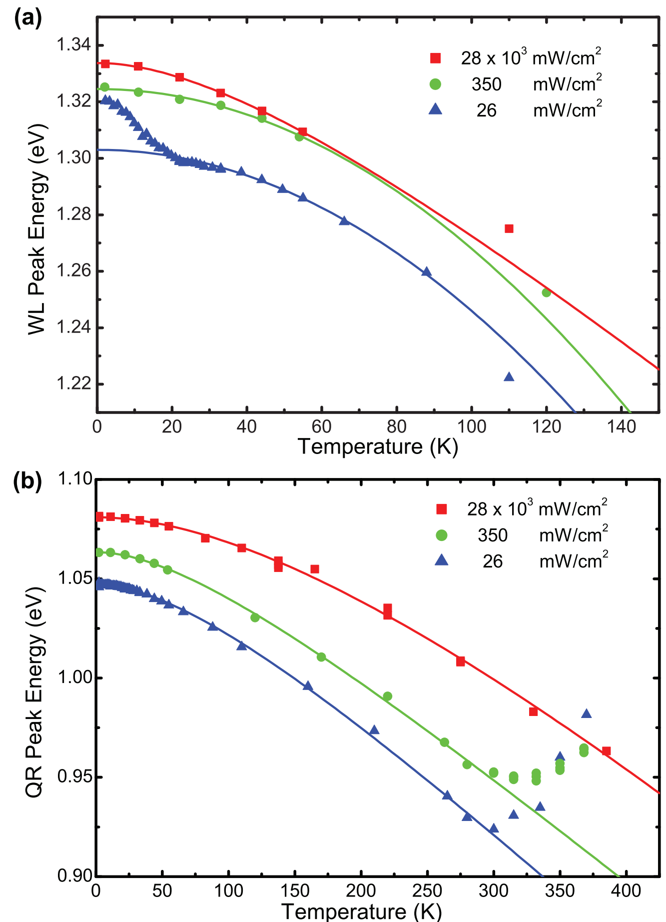


FIG. 4. (Color online) Temperature varying PL data for (a) the WL and (b) QR peaks at three different laser powers. The lines are fits to the Varshni expression for temperatures <300 K (Ref. 33).

Similar data, but for the QR peak, is shown in Fig. 3(b). At low temperatures the typical blueshift with increasing laser power is observed. This is followed by a slight increase of the blueshift as the temperature is raised all the way to 300 K. Then, quite remarkably, and in contrast to the WL, an initial redshift begins to become visible above 340 K. As the temperature is increased further, the magnitude of the initial redshift increases, as does the critical laser power before the emission begins to blueshift. This redshift is also very large, having a magnitude of ∼35 meV at 400 K, which is comparable to the 50-meV blueshift at 2 K. This shows that at temperatures above 340 K, the acceptor holes migrate to the QRs.

The temperature-varying PL scans at three different incident laser powers are shown in Fig. 4. As seen in the previous power varying data, the WL shows unusual behavior below 20 K only at low laser powers. In Fig. 4(a), a rapid redshift is seen in the 26 mW/cm$^2$ data as the temperature increases up to 20 K. Above this temperature, the peak resumes a typical Varshni-shaped dependence.[33] At higher laser powers, the WL peak shows Varshni dependence over the entire temperature range. This can again be explained by the presence of acceptor holes: at temperatures below 20 K the acceptor holes are present in the WL but only at low incident laser powers. As the temperature is increased, the acceptor holes are thermally excited out of the WL, until by 20 K they are no longer present. At higher laser powers this unusual behavior is no longer observed as the acceptor states are effectively screened by the high carrier density. The Varshni equation provides an empirical description of the variation in the band gap,[33] with parameters that are well known for bulk semiconductors, e.g., for bulk GaAs and GaSb the band gap decreases by 30.8 meV[34] and 31.7 meV,[35] respectively, from 0 to 140 K. The magnitude of the temperature-induced energy shift of the WL PL in this sample is much larger than these values at all laser powers. As can clearly be seen in Fig. 4, the Varshni curves, and therefore the Varshni parameters, are not the same at different laser powers. In general, Varshni parameters for QDs, and in particular for type-II heterostructures, are not well established, so it is difficult to comment on this further. However, for the purposes of this investigation, it is sufficient to note the Varshni shape (i.e., parabolic at low temperature and linear at high temperature) is observed for all laser powers except the 26 mW/cm$^2$ temperature data, where the discharging of the WL occurs at low temperatures.

In contrast to the WL, the QR peak shows a typical Varshni shift up to ∼300 K at all laser powers [Fig. 4(b)]. It is only above this temperature that the effects of the acceptor holes become apparent: acceptor holes migrate into

the QRs as the temperature is increased. The increase in QR occupancy and hence the magnitude of the high-temperature blueshift at different laser powers is directly controlled by the photogeneration rate through OICD. Thus the magnitude of the blueshift is reduced at higher incident laser powers until no blueshift is seen at the highest laser power.

Effectively, both Figs. 3 and 4 show the same phenomena but from two different perspectives. The power-varying data of Fig. 3 directly demonstrates the OICD effect in both the WL and QRs at different temperatures. This figure also shows that at low (or zero) laser powers, significant numbers of acceptor holes are present in the sample (as also evidenced by the GaAs related peaks in Fig. 2). Figure 4 further demonstrates migration of these acceptor holes from the WL at $\leqslant$20 K to the QRs at $\geqslant$300 K. Fluctuations in the WL valence band edge, due to sample inhomogeneity during growth, accounts for the localization of acceptor holes below 20 K. Above this temperature, thermal excitation is sufficient to allow dopant holes to migrate into the more deeply confining QD/QRs. However, our PL spectra do not reveal the location of the acceptor holes in the 20–300 K range. A likely explanation is the presence of dark dot states in the sample. XTEM images of GaSb/GaAs samples have shown that large single-lobed GaSb structures (QDs) have much more strain in the surrounding GaAs matrix than smaller double-lobed structures (QRs).[30] This high strain is further evidenced by the tendency for screw dislocations to form in the GaAs layer above the QDs.[31] Calculations of the band structure of different sized GaSb/GaAs QDs have shown that for large, highly strained QDs, there is a significant increase in the conduction band minimum energy of the GaAs close to the QD.[36] Therefore, gradients in the GaAs conduction band minimum may lead to strong electron repulsion from the highly strained QDs in this sample, hindering radiative recombination and leading to dark dots. Conversely, it is established that QR formation is very effective at relaxing the strain,[37] hence producing a lower gradient in the GaAs conduction band, allowing greater electron-hole wave-function overlap. Indeed, the magneto-PL measurements of Ref. 30 found that differences in growth conditions, and thus QR morphologies, can tune the excitonic properties of such nanostructures. It was shown that QRs with larger inner radii have less strain in the surrounding GaAs, allowing electrons much closer to the holes in the QRs. Therefore, electron-hole interactions dominate, and, as the incident laser power was increased, the excitonic binding increased. In contrast, for QRs with smaller inner radii (more QD-like), increased strain in the GaAs above the QR leads to a strong electron-electron interaction. Consequently, as the incident laser power was increased for these QRs, the screening dominated and the excitonic binding decreased. Extending this argument a little further we propose that, broadly speaking, the QDs in our sample are dark and the QRs are bright.[38] The disappearance of the acceptor holes in the intermediate temperature range is then explained by their migration into the dark QDs. Bright QRs would be difficult to charge because holes are efficiently removed by recombination, whereas dark dots will retain their charge. Dark dots thus provide a hidden reservoir for the acceptor holes with a deep localization potential. When the temperature is high enough for the holes to escape from the dark dots, thermalization occurs, transferring acceptor holes from the dots to the rings. The fact that this thermalization is only seen at the anomalously high temperature of 320 K is directly attributable to the large localization energy of holes in GaSb/GaAs QDs/QRs (~600 meV for the ground state[6,7]).

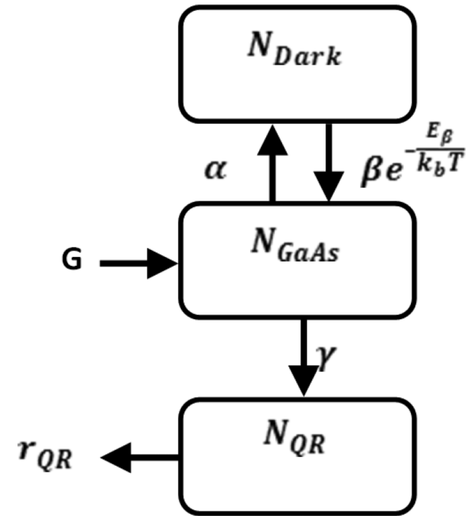


FIG. 5. Block diagram to illustrate hole migration in the modeled system.

## V. MODELING

A simple rate equation model was created (Fig. 5) to replicate the OICD effect using the following equations:

$$\frac{dN_{\rm GaAs}}{dt} = G - \gamma N_{\rm GaAs} - \alpha N_{\rm GaAs}\left(N_{\rm Dark}^{\rm Max} - N_{\rm Dark}\right) + \beta e^{-\frac{E_\beta}{k_b T}} N_{\rm Dark}, \quad (1)$$

$$\frac{dN_{\rm QR}}{dt} = \gamma N_{\rm GaAs} - r_{\rm QR} n_e N_{\rm QR}, \quad (2)$$

$$\frac{dN_{\rm Dark}}{dt} = \alpha N_{\rm GaAs}\left(N_{\rm Dark}^{\rm Max} - N_{\rm Dark}\right) - \beta e^{-\frac{E_\beta}{k_b T}} N_{\rm Dark}, \quad (3)$$

where $N_{\rm GaAs}$, $N_{\rm QR}$, and $N_{\rm Dark}$ are the number of holes in the GaAs, QRs, and dark QDs, respectively. $N_{\rm Dark}^{\rm Max}$ is the maximum average hole occupancy of dark QDs per QR. Hence if the QD density in the sample is lower than the QR density, $N_{\rm Dark}^{\rm Max}$ will be less than the maximum occupancy of a QD. $\alpha$, $\beta$, and $\gamma$ are constants that describe the probability of holes moving between respective regions. $E_\beta$ is the activation energy for the thermalization of holes from the dark QDs, $G$ is the photogenerated carrier rate, $r_{\rm QR}$ is a constant related to electron-hole recombination in the QRs, and $n_e$ is the total number of photogenerated electrons in the system. From charge neutrality conditions, $n_e = N_{\rm GaAs} + N_{\rm QR} + N_{\rm Dark} - N_A$, where $N_A$ is the number of acceptors in the GaAs. These equations model the movement of holes through the different structures in the sample. To keep the model simple and to elucidate the physics in which we are interested, photogenerated electrons are assumed to instantaneously reach, and interact exclusively with, the QRs.

Eqs. (1)–(3) were solved for $N_{\rm QR}$ assuming steady state conditions, i.e., left-hand side of equations set to zero. $N_{\rm QR}$

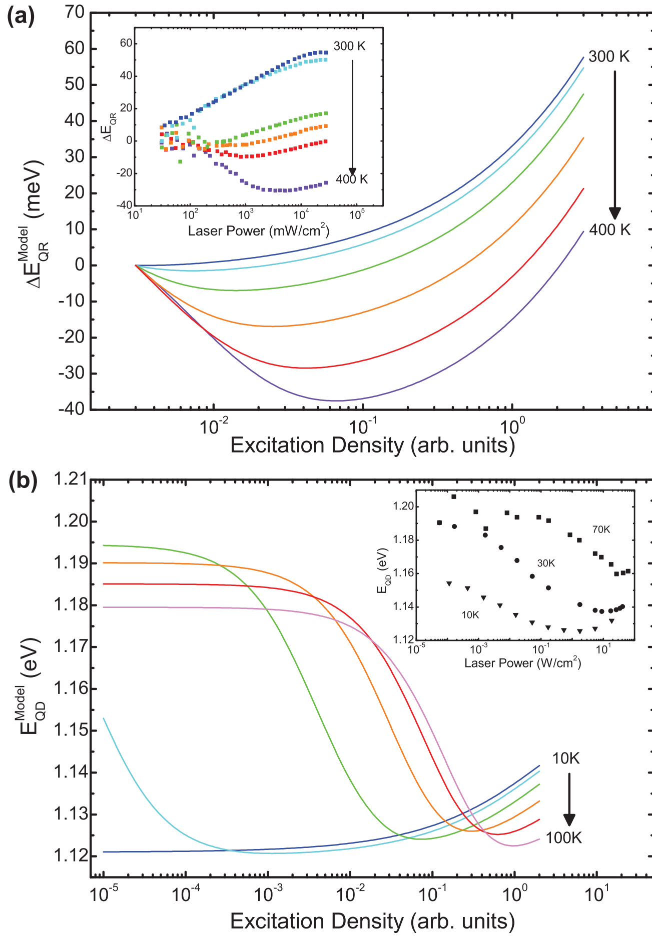


FIG. 6. (Color online) (a) Predicted QR emission energy shifts as a function of excitation density at different temperatures for the sample presented here. The inset shows the sample's actual PL data for comparison with the model output. (b) The absolute energy for a MOCVD grown QD sample, as predicted by the model. The inset shows the MOCVD grown sample's PL data taken from Ref. 27.

was converted into an energy shift of the ground state PL (which remains responsible for the emission, even when dots are charged[26]) by assuming a capacitive charging energy of 24 meV per additional carrier after the first.[38] Bulk GaSb Varshni parameters were used to calculate changes in the bandgap energy at different temperatures. Output from the model is shown in Fig. 6, and the free parameters used to generate this output are shown in Table I. The value of $E_\beta$ used is consistent with values that have been previously measured in GaSb/GaAs QDs.[7] It can be seen that our model successfully replicates the general behavior of OICD seen in this MBE-grown sample [Fig. 6(a) inset]. The evolution of the redshift of the QR emission occurs over the same temperature range as the sample and also over the same variation of order of magnitude of excitation density. The magnitude of the initial redshift seen at higher temperatures and the magnitude of the blueshift at lower temperatures are accurately replicated by the model.

The WL has not been included as this would vastly complicate the model and also introduce further free parameters. We have also neglected the capacitive charging of the dark QDs from multiple hole occupation, which would change $E_\beta$.

TABLE I. Values used in the model to give the data shown in Fig. 6 for both the MBE-grown sample presented here and for the MOCVD-grown sample published in Ref. 27. Note that for the MBE sample, parameters $\beta$ and $E_\beta$ describe the properties of dark QDs, while for the MOCVD-grown sample of Ref. 27 they describe the properties of the acceptors. Also, $N_{\mathrm{Dark}}^{\mathrm{Max}}$ is only used for the MBE sample as dark QDs are not included in the MOCVD model. The order of magnitude of parameters $\alpha,\beta,\gamma$, and $r_{\mathrm{QR}}$ is arbitrary.

| | MBE Sample | MOCVD sample (Ref. 27) |
|---|---|---|
| $\alpha$ | 0.05 $s^{-1}$ | 0.1 $s^{-1}$ |
| $\beta$ | 50 $s^{-1}$ | 0.20 $s^{-1}$ |
| $E_\beta$ | 475 meV | 21.6 meV |
| $\gamma$ | 7 $s^{-1}$ | 1 $s^{-1}$ |
| $N_{\mathrm{Dark}}^{\mathrm{Max}}$ | 3 | – |
| $N_A$ | 3 | 6 |
| $r_{\mathrm{QR}}$ | 0.40 $s^{-1}$ | 0.35 $s^{-1}$ |
| $\Delta E_{CC}$ | 24 meV | 13 meV[a] |

[a]References 25 and 27.

This could be introduced by modifying the exponential terms in Eqs. (1) and (3) to include an $N_{\mathrm{Dark}}$ dependence but doing so prevents analytical solutions to the simultaneous equations and would require numerical methods to obtain a solution. To a large extent, the phenomenon of the dark QDs becoming harder to fill at higher occupancy is already present in the model with the inclusion of the $N_{\mathrm{Dark}}^{\mathrm{Max}}$ term. We believe that the simpler model presented here, which demonstrates all the important phenomena, is preferable to a more complex model containing many more free parameters.

There are several free parameters that account for the majority of the OICD effects produced by the model. An important process in OICD is the occupation of intermediate hole reservoirs (the dark QDs), which provide states at energies that are higher than those of the QN responsible for the PL (bright QRs). Here, the dark QDs provide states at higher energy because they are occupied by more holes than the QRs, a direct consequence of their dark character. The role of the hole reservoir is to delay the movement of photogenerated holes to the recombination center (bright QRs), such that the latter are discharged by recombination with photogenerated electrons. OICD is thus a dynamic equilibrium effect. The inflection point occurs when these dark QDs become saturated, and the excess photogenerated holes spill into the QRs, leading to a blueshift. If the dark QDs are more easily saturated, then the inflection point will occur at a lower laser power; thus, over a given laser power range, the magnitude of the initial redshift will be decreased. Indeed, this effect causes the changes in the model's output at different temperatures. At low temperatures, $e^{-E_\beta/k_bT}$ is smaller (the dark QDs are more easily saturated); thus, the inflection point occurs at lower laser power, and the magnitude of the redshift seen over the laser power range is decreased. Increasing the number of acceptors, $N_A$, increases the magnitude of the initial redshift (there are more holes at low laser power to charge the QRs), and the inflection point shifts to higher laser power (more photogenerated electrons are required to depopulate the QRs of acceptor holes).

Further support for our model comes from the fact that it can be adapted to replicate the OICD behavior seen in

GaSb/GaAs QDs grown by metal organic chemical vapor deposition (MOCVD)[27] [Fig. 6(b)]. To do this, $N_{\mathrm{Dark}}$ was renamed to $N_A^{\mathrm{Occupied}}$(the number of acceptor states occupied by holes), and $N_{\mathrm{Dark}}^{\mathrm{Max}}$ was replaced by $N_A$. Essentially the physics of the system remains the same as previously stated, but the acceptor states take the role of the dark QDs. The free parameters used in the model are shown in Table I. Compared to the parameters used for the MBE-grown sample, $E_\beta$ was decreased to reflect the confining potential of the acceptor states, and $N_A$ increased due to the higher acceptor density expected in MOCVD grown samples. The magnitude of the energy shifts and the behavior predicted by the model matches the data very well.

## VI. CONCLUSIONS

Optically induced charge depletion has been observed in both the WL and QRs of a GaSb/GaAs heterostructure but in different temperature regimes. Thermal quenching of OICD in the WL indicates a migration of acceptor holes out of this region as the temperature was increased from 2 to 20 K, while the emergence of OICD at temperatures above 300 K in the QRs clearly demonstrates charging of these nanostructures above room temperature. Thus observations of OICD were used to follow the movement of acceptor holes between the different nanostructures within the sample. The presence of highly strained dark QDs is invoked to explain the location of acceptor holes at intermediate temperatures (20–300 K) and is strongly supported by a rate equation model that successfully replicates the temperature and laser excitation power dependence of the PL energy both for the data presented here and for that published in Ref. 27. The preferential occupation of the QRs at high temperatures (>300 K) indicates that the large confining potential of these nanostructures is sufficient to trap holes. This is promising for the implementation of GaSb/GaAs QRs in devices such as lasers or memories, which typically operate at or above room temperature.

## ACKNOWLEDGMENTS

This work was supported by the EPSRC in the framework of the QD2D project (Grant No. EP/H006419), by the Royal Society—Brian Mercer Feasibility Award and QinetiQ (Agreement No. 3000127730).

*Corresponding author: p.hodgson1@lancaster.ac.uk

[1] D. Bimberg, M. Grundmann, and N. Ledentsov, *Quantum Dot Heterostructures* (Wiley, New York, 1999).
[2] T. Y. Gu, M. A. El-Emawy, K. Yang, A. Stintz, and L. F. Lester, Appl. Phys. Lett. **95**, 261106 (2009).
[3] A. J. Shields, Nat. Photonics **1**, 215 (2007).
[4] R. B. Laghumavarapu, A. Moscho, A. Khoshakhlagh, M. El-Emawy, L. F. Lester, and D. L. Huffaker, Appl. Phys. Lett. **90**, 173125 (2007).
[5] P. J. Carrington, A. S. Mahajumi, M. C. Wagener, J. R. Botha, Q. Zhuang, and A. Krier, Physica B **407**, 1493 (2012).
[6] T. Nowozin, A. Marent, L. Bonato, A. Schliwa, D. Bimberg, E. P. Smakman, J. K. Garleff, P. M. Koenraad, R. J. Young, and M. Hayne, Phys. Rev. B **86**, 035305 (2012).
[7] T. Nowozin, L. Bonato, A. Hogner, A. Wiengarten, D. Bimberg, W.-H. Lin, S.-Y. Lin, C. J. Reyner, B. L. Liang, and D. L. Huffaker, Appl. Phys. Lett. **102**, 052115 (2013).
[8] M. Geller, A. Marent, T. Nowozin, D. Bimberg, N. Akcay, and N. Oncan, Appl. Phys. Lett. **92**, 092108 (2008).
[9] A. Marent, T. Nowozin, M. Geller, and D. Bimberg, Semicond. Sci. Technol. **26**, 014026 (2011).
[10] M. Hayne, R. J. Young, E. P. Smakman, T. Nowozin, P. Hodgson, J. K. Garleff, P. Rambabu, P. M. Koenraad, A. Marent, L. Bonato, A. Schliwa, and D. Bimberg, J. Phys. D: Appl. Phys. **46**, 264001 (2013).
[11] E. Ribeiro, A. O. Govorov, W. Carvalho, and G. Medeiros-Ribeiro, Phys. Rev. Lett. **92**, 126402 (2004).
[12] I. L. Kuskovsky, W. MacDonald, A. O. Govorov, L. Mourokh, X. Wei, M. C. Tamargo, M. Tadic, and F. M. Peeters, Phys. Rev. B **76**, 035342 (2007).
[13] I. R. Sellers, V. R. Whiteside, I. L. Kuskovsky, A. O. Govorov, and B. D. McCombe, Phys. Rev. Lett. **100**, 136405 (2008).
[14] B. Bansal, M. Hayne, M. Geller, D. Bimberg, and V. V. Moshchalkov, Phys. Rev. B **77**, 205317 (2008).
[15] L. Muller-Kirsch, R. Heitz, A. Schliwa, O. Stier, D. Bimberg, H. Kirmes, and W. Neumann, Appl. Phys. Lett. **78**, 3908 (2001).
[16] B. Bansal, S. Godefroo, M. Hayne, G. Medeiros-Ribeiro, and V. V. Moshchalkov, Phys. Rev. B **80**, 205317 (2009).
[17] K. Gradkowski, T. J. Ochalski, D. P. Williams, S. B. Healy, J. Tatebayashi, G. Balakrishnan, E. P. O'Reilly, G. Huyet, and D. L. Huffaker, Phys. Status Solidi B **246**, 752 (2009).
[18] J. Tatebayashi, A. Khoshakhlagh, S. H. Huang, G. Balakrishnan, L. R. Dawson, and D. L. Huffaker, Appl. Phys. Lett. **90**, 261115 (2007).
[19] Y. S. Chiu, M. H. Ya, W. S. Su, and Y. F. Chen, J. Appl. Phys. **92**, 5810 (2002).
[20] F. Hatami, M. Grundmann, N. N. Ledentsov, F. Heinrichsdorff, R. Heitz, J. Bohrer, D. Bimberg, S. S. Ruvimov, P. Werner, V. M. Ustinov, P. S. Kop'ev, and Z. I. Alferov, Phys. Rev. B **57**, 4635 (1998).
[21] D. Alonso-Alvarez, B. Alen, J. M. Garcia, and J. M. Ripalda, Appl. Phys. Lett. **91**, 263103 (2007).
[22] P. J. Simmonds, R. B. Laghumavarapu, M. Sun, A. D. Lin, C. J. Reyner, B. L. Liang, and D. L. Huffaker, Appl. Phys. Lett. **100**, 243108 (2012).
[23] Y. I. Mazur, V. G. Dorogan, G. J. Salamo, G. G. Tarasov, B. L. Liang, C. J. Reyner, K. Nunna, and D. L. Huffaker, Appl. Phys. Lett. **100**, 033102 (2012).
[24] K. Gradkowski, T. J. Ochalski, N. Pavarelli, H. Y. Liu, J. Tatebayashi, D. P. Williams, D. J. Mowbray, G. Huyet, and D. L. Huffaker, Phys. Rev. B **85**, 035432 (2012).
[25] M. Geller, C. Kapteyn, L. Muller-Kirsch, R. Heitz, and D. Bimberg, Appl. Phys. Lett. **82**, 2706 (2003).

[26] P. D. Hodgson, R. J. Young, M. A. Kamarudin, P. J. Carrington, A. Krier, Q. D. Zhuang, E. P. Smakman, P. M. Koenraad, and M. Hayne, J. Appl. Phys. **114**, 073519 (2013).

[27] M. Hayne, O. Razinkova, S. Bersier, R. Heitz, L. Muller-Kirsch, M. Geller, D. Bimberg, and V. V. Moshchalkov, Phys. Rev. B **70**, 081302 (2004).

[28] A. S. Chaves, A. F. S. Penna, J. M. Worlock, G. Weimann, and W. Schlapp, Surf. Sci. **170**, 618 (1986).

[29] M. Hayne, A. Usher, A. S. Plaut, and K. Ploog, Phys. Rev. B **50**, 17208 (1994).

[30] M. A. Kamarudin, M. Hayne, R. J. Young, Q. D. Zhuang, T. Ben, and S. I. Molina, Phys. Rev. B **83**, 115311 (2011).

[31] E. P. Smakman, J. K. Garleff, R. J. Young, M. Hayne, P. Rambabu, and P. M. Koenraad, Appl. Phys. Lett. **100**, 142116 (2012).

[32] O. Madelung, *Semiconductors: Data Handbook* (Springer, New York, 2004).

[33] Y. P. Varshni, Physica **34**, 149 (1967).

[34] J. S. Blakemore, J. Appl. Phys. **53**, R123 (1982).

[35] M. C. Wu and C. C. Chen, J. Appl. Phys. **72**, 4275 (1992).

[36] M. Hayne, J. Maes, S. Bersier, V. V. Moshchalkov, A. Schliwa, L. Muller-Kirsch, C. Kapteyn, R. Heitz, and D. Bimberg, Appl. Phys. Lett. **82**, 4355 (2003).

[37] P. J. Carrington, R. J. Young, P. D. Hodgson, A. M. Sanchez, M. Hayne, and A. Krier, Crystal Growth & Design **13**, 1226 (2013).

[38] R. J. Young, E. P. Smakman, A. M. Sanchez, P. Hodgson, P. M. Koenraad, and M. Hayne, Appl. Phys. Lett. **100**, 082104 (2012).